Phys Chem Minerals (2011) 38:685–691
DOI 10.1007/s00269-011-0441-4

ORIGINAL PAPER

Raman spectra of bixbyite, Mn_2O_3, up to 40 GPa

S.-H. Shim · D. LaBounty · T. S. Duffy

Received: 15 March 2011 / Accepted: 25 May 2011 / Published online: 12 June 2011

Abstract The Raman spectra of bixbyite, Mn_2O_3, were measured up to 40 GPa at room temperature. Mn_2O_3 undergoes a phase transition from the C-type rare earth structure to the $CaIrO_3$-type (post-perovskite) structure at 16–25 GPa. The transition pressure measured in Raman spectroscopy is significantly lower than the pressure reported previously by an X-ray diffraction study. This could be due to the greater polarizability in the $CaIrO_3$-type structure, consistent with high-pressure observation on the $CaIrO_3$ type in $MgGeO_3$, although it is still possible that experimental differences may cause the discrepancy. Unlike the change at the perovskite to $CaIrO_3$-type transition, the spectroscopic Grüneisen parameter does not decrease at the C-type to $CaIrO_3$-type transition. The spectroscopic Grüneisen parameter of the low-pressure phase (C type) is significantly lower than thermodynamic Grüneisen parameter, suggesting significant magnetic contributions to the thermodynamic property of this material. Our Raman measurements on $CaIrO_3$-type Mn_2O_3 contribute to building systematic knowledge about this structure, which has emerged as one of the common structures found in geophysically important materials.

Keywords Raman spectroscopy · Mn_2O_3 · Phase transition · Grüneisen parameter

S.-H. Shim (✉) · D. LaBounty
Massachusetts Institute of Technology, 77 Massachusetts Avenue, Cambridge, MA 02139, USA
e-mail: sangshim@mit.edu

T. S. Duffy
Princeton University, Guyot Hall, Princeton, NJ 08544, USA

Introduction

Understanding the high-pressure behavior of sesquioxides (M_2O_3, M = Fe, Mn, Al, Cr, etc) is important in geophysics and high-pressure physics. For example, Cr-doped Al_2O_3, i.e., ruby, has been extensively used as a pressure standard at high pressure (Piermarini et al. 1975; Mao et al. 1986). Pressure calibration of the ruby scale can be affected by phase transitions (Funamori and Jeanloz 1997; Duan et al. 1998; Lin et al. 2004; Shim et al. 2004b). Also, many of the 3*d* transition metals may exist in the mantle as minor elements, and their sesquioxides appear to have pressure–temperature stability fields for phases which also occur in mantle silicates (e.g., $MgSiO_3$). For example, Fe_2O_3, Al_2O_3, and Mn_2O_3 have stability fields for the $CaIrO_3$-type (post-perovskite) structure (Ono et al. 2004; Oganov and Ono 2005; Santillán et al. 2006; Shim et al. 2009), which has been found to be stable in (Mg,Fe)(Al,Si)O_3 at the pressure–temperature conditions of the lowermost mantle of Earth (Murakami et al. 2004; Oganov and Ono 2004; Shim et al. 2004a; Catalli et al. 2009).

Unlike Fe_2O_3 and Al_2O_3 where the stability field of the $CaIrO_3$-type phase appears after either perovskite or Rh_2O_3-II phase, Mn_2O_3 undergoes a phase transition from the C-type rare earth structure (hereafter "C type") to the $CaIrO_3$ type at 27–38 GPa (Yamanaka et al. 2005; Santillán et al. 2006). It is also interesting to point out that the transition to the post-perovskite phase occurs at room temperature in Mn_2O_3. This is likely due to the structural similarities between the two phases as pointed out by Santillán et al. (2006).

Raman spectroscopy provides an alternative tool to study phase transitions. Unlike X-ray diffraction where the number of electrons determines the diffraction intensity, Raman intensities are controlled by polarizability (Fadini

and Schnepel 1989). A previous study of $MgGeO_3$ found that the Raman intensity is much stronger in the $CaIrO_3$-type phase than the perovskite-type phase (Shim et al. 2007). Therefore, it is of interest to determine whether a similar relationship holds with the transition from the C-type phase. In addition, Raman spectroscopy can provide constraints on Grüneisen parameters (Williams et al. 1987; Lu and Hofmeister 1994; Chopelas 1996; Gillet et al. 1998). In case of solids with significant magnetic and electronic contributions, high-pressure Raman measurements can constrain the pure phonon contributions to the thermal properties of a solid, which are not easily accessible with other techniques (Shim and Duffy 2002). Previous studies have shown that the Grüneisen parameter decreases at the perovskite to post-perovskite phase transition in $MgSiO_3$, $MgGeO_3$, and $CaIrO_3$ (Shim et al. 2007, 2008; Hustoft et al. 2008). Therefore, it is also of interest if this is the case for the phase transition from the C-type phase to the $CaIrO_3$-type phase.

In this paper, we report Raman scattering measurements of Mn_2O_3 up to 40 GPa under quasi-hydrostatic stress conditions. Our results provide new constraints on the phase transition and thermal properties of Mn_2O_3 at high pressure.

Experimental method

Synthetic Mn_2O_3 (Aldrich, purity 99%) was used in powder form. We confirmed the quality using powder X-ray diffraction and Raman spectroscopy at ambient conditions. The same sample material was also used in Santillán et al. (2006). Thin platelets of Mn_2O_3 powder were made by cold compressing the material in a moissanite anvil cell. The sample was loaded in 250-μm-diameter holes in stainless steel gaskets. Low-fluorescence diamond anvils with 500-μm culets compressed the sample using symmetric diamond-anvil cells. Argon was loaded cryogenically as a pressure transmitting medium. The data between 0 and 9 GPa were collected with NaCl as a medium.

The sample foil was loaded in direct contact with one of the diamond anvils, and spectra were measured from this side (Fig. 1). Because diamond is an excellent thermal conductor, this setup reduces the heating of the sample by the laser beam. In order to prevent bridging of the sample between the anvils, we placed spacers on the opposite side of the sample to ensure a gap that allows Ar to flow between the sample and the anvil. The spacer grains were also Mn_2O_3.

Even with this setup, we found that high-intensity laser beam can cause some changes in the Raman spectra. A 100-mW laser beam focused on the sample in the diamond-anvil cell at low pressure produced some new peaks if an

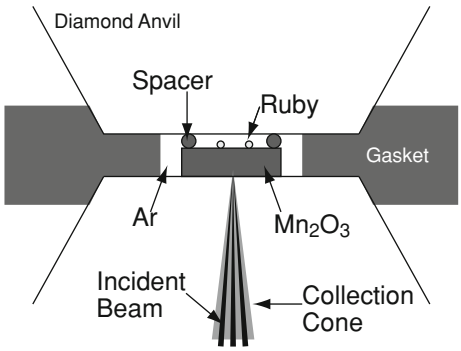

Fig. 1 Schematic diagram of the sample setup in the diamond-anvil cell

NaCl medium is used (Fig. 2j). The intensities of these peaks increase with time. The wavenumbers and intensities of the new peaks are consistent with those of MnO_2 (Buciuman et al. 1999), indicating that high-intensity laser beam can oxidize Mn_2O_3 into MnO_2 (Fig. 2j). This is, perhaps, due to the surface reaction between Mn_2O_3 and oxygen, captured during loading under atmosphere, under intense laser beam focused on a small area. It is notable that Raman intensity of Mn_2O_3 is much smaller than that of MnO_2 (Buciuman et al. 1999), and therefore, even small production of MnO_2 would change the measured spectra significantly (Fig. 2j). In order to avoid the laser-induced reaction, we measured the Raman spectra of the samples in the diamond-anvil cell by varying the power of the laser beam. We found that a laser power of 10–20 mW does not change the spectrum of Mn_2O_3 for 3 hours. In this study, we used the spectra that do not have any evidence of the laser-induced reaction.

Three to four ruby chips were loaded at various sample positions for pressure determination using the quasi-hydrostatic ruby scale (Mao et al. 1986). All ruby grains were loaded on the opposite side of the sample surface from which we measured Raman spectra. Because Mn_2O_3 remains opaque throughout the examined pressure range, no signal from ruby is observed in our spectra. Pressures measured from different ruby grains did not differ more than ±1 GPa, indicating homogeneity in stress condition.

Four different sets of measurements were conducted with two different Raman systems. The micro-Raman system at Princeton University consists of a 200 mW Ar-ion laser, 0.5 m single spectrometer, charge-coupled device (CCD) detector (1,100 × 330 pixels), and holographic optics. The focal spot size was 10–20 μm. The micro-Raman system at MIT consists of a 1.2 W Kr/Ar-mixed ion laser, 0.5 m single spectrometer, CCD detector (1,300 × 100 pixels), and holographic optics. The focal spot is 2 μm in this system. We used a 514.532 nm laser wavelength for Raman scattering. The results from the two instruments are identical to each other.

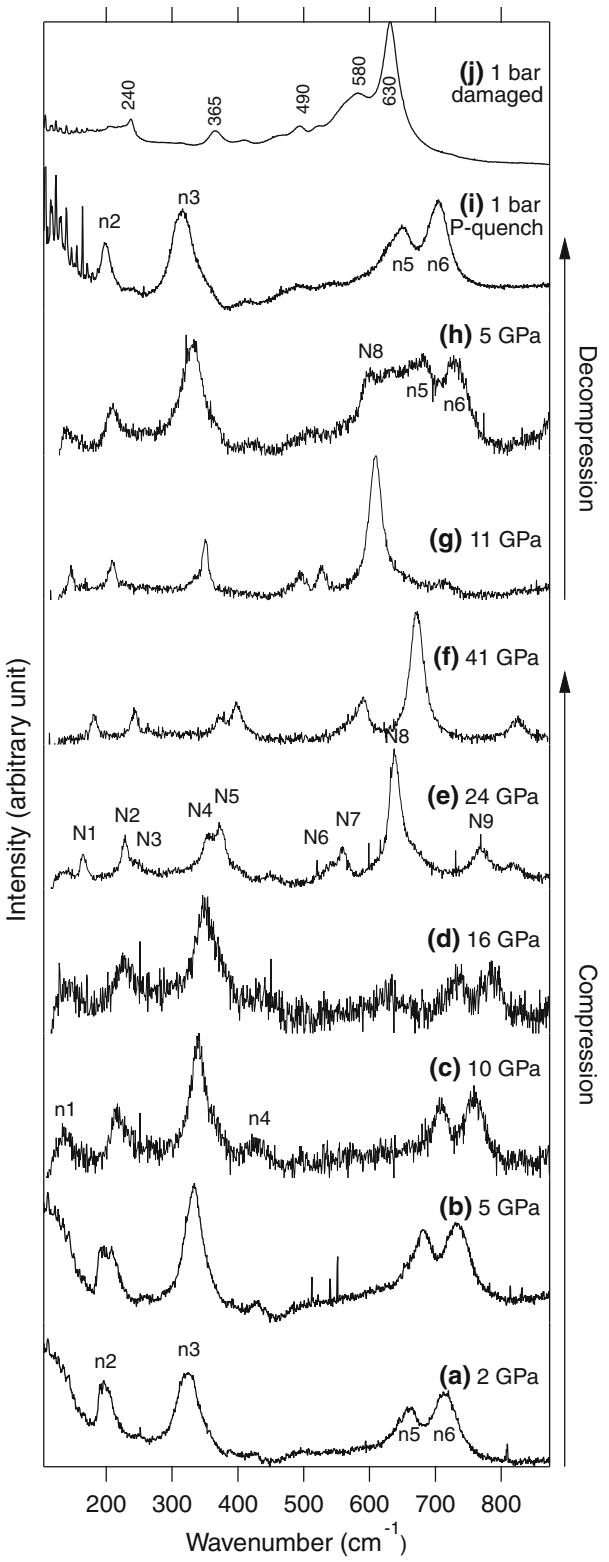

Fig. 2 Raman spectra of Mn_2O_3 measured during compression (**a**–**f**) and decompression (**g**– **i**). The modes were tentatively assigned in the order of their frequencies for the C-type phase (n_1–n_6) and for the $CaIrO_3$-type phase (N_1–N_9). A spectrum measured under intense laser illumination at 1 bar is shown in **j** for comparison. In **j**, we present the wavenumbers of the observed peaks

A spectral range of 100–900 cm^{-1} was measured. The spectrometer was calibrated using the neon emission spectrum. The precision of the measured frequency is better than ± 1 cm^{-1}. An exposure time of 10–30 minutes was used.

Results and Discussion

The C-type phase has a cubic structure $(Ia\bar{3})$ and is expected to have 22 Raman-active phonon modes (White and Keramidas 1972). Mn_2O_3 transforms from an orthorhombic (distorted C type) structure to a cubic (C type) structure at 302 K (Grant et al. 1968; Geller 1971). Although the temperature of laboratory was maintained to be 293 K, it is possible that the temperature of the Mn_2O_3 sample might be slightly higher and within the stability field of the cubic phase due to slight heating by laser illumination. In addition, it is thought that pressure may suppress the distortion (Prewitt et al. 1969).

We observed a total of 4 Raman modes (n_2, n_3, n_5, and n_6) at pressures below 5 GPa between 100 and 900 cm^{-1} (Fig. 2a). With compression, the peak at 426 cm^{-1} (n_4) gains intensity (Fig. 2b). A large background structure was observed at wavenumbers below 150 cm^{-1} at pressures lower than 10 GPa. However, the structure disappears with compression and becomes weak enough to reveal a peak at 137 cm^{-1} (n_1). Therefore, we observed a total of 6 modes within the stability field of the C type. Although this is far less than theoretical predictions (White and Keramidas 1972), our observation is generally in agreement with previous Raman reports on α-Mn_2O_3. White and Keramidas (1972) reported three peaks at 565, 620, and 672 cm^{-1}. The latter two appear to be in agreement with our n_5 and n_6, whereas we do not observe any peaks between 500 and 600 cm^{-1} within the stability field of the C type. Kapteijin et al. (1994) reported three peaks at 311, 653, and 697 cm^{-1}, all of which are observed in our study. In addition to these three modes, Buciuman et al. (1999) observed a weak mode at 360–390 cm^{-1}. Although we do not observe any peak near this wavenumber range at 1 bar, n_4 gains significant intensity with pressure near this wavenumber range (Fig. 2a–c). Lack of previous reports on n_1 and n_2 is, perhaps, due to the fact that the low wavenumber range was not explored in the previous studies. It is also important to mention that high-quality Raman measurements are challenging for opaque materials such as Mn_2O_3.

Beginning from 16 GPa, we found severe changes in the Raman spectra of Mn_2O_3 (Fig. 2d). A peak appears at 626 cm^{-1} (N_8) and gains intensity with compression. This peak ultimately becomes the most intense peak for the

high-pressure phase of Mn_2O_3. Two new peaks appear at 530–550 cm^{-1} (N_6 and N_7), and two low-pressure phase peaks (n_2 and n_3) split into $N_2 + N_3$ and $N_4 + N_5$, respectively (Figs 2d, e and 3). The wavenumber of n_1 appears to show a discontinuous increase at the phase transition (Fig. 3). Two low-pressure features disappear at the phase transition (n_4 and n_6). n_5 appears to survive through the phase transition and continues up to the maximum pressure of this study (N_9).

Caracas and Cohen (2006) showed that 12 modes among a total of 30 modes are Raman active for the $CaIrO_3$-type (*Cmcm*) structure. In this study, we identify a total of 9 modes in Mn_2O_3 between 100 and 900 cm^{-1} (Fig. 2e). In $MgGeO_3$, a total of 10 modes were found in the Raman spectra of the $CaIrO_3$ type between 100 and 900 cm^{-1} (Shim et al. 2007). In Fig. 2 of Hustoft et al. (2008), we compared the Raman spectra of the $CaIrO_3$-type phase between $MgGeO_3$ and Mn_2O_3. Striking similarity can be found between these two materials. In contrast, only 5 modes were found for $CaIrO_3$ itself (Hustoft et al. 2008).

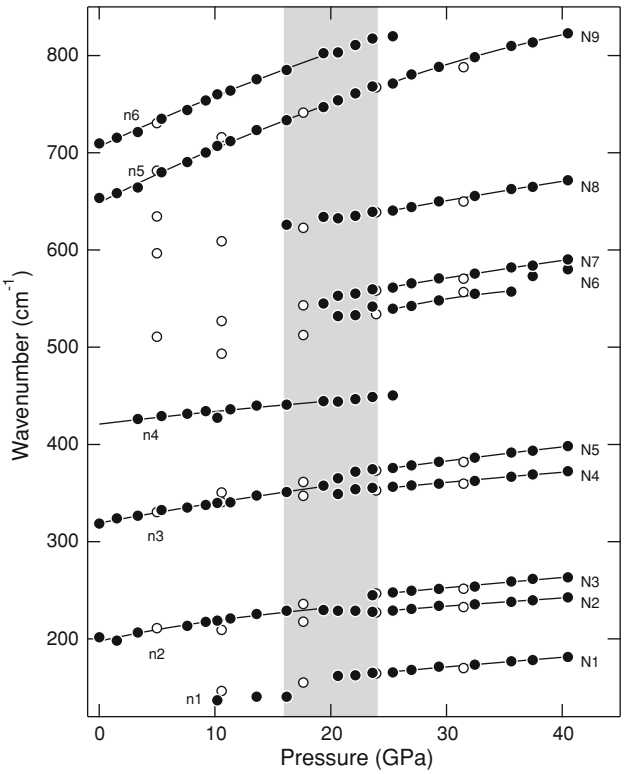

Fig. 3 Pressure-induced shifts of the Raman modes of Mn_2O_3. *Solid and open symbols* represent data points measured during compression and decompression, respectively. Fitting of the data is shown by *curves*. The size of *error bar* for mode frequency is smaller than that of the symbols. Uncertainty in pressure is 3%. The *gray area* indicates where the phase transition was observed. The compression data below and above 9 GPa were measured using a NaCl medium and an Ar medium, respectively

This is perhaps related to the very different bonding characters in $CaIrO_3$, compared with $MgGeO_3$ and Mn_2O_3.

It is important to make sure that the new peaks observed at high pressure are not from the reaction by the illumination of intense laser beam. As discussed earlier, we investigate threshold laser intensity to prevent laser-induced reaction of the sample. MnO_2, a possible oxidation product by laser-induced reaction as found in our test measurements (Fig. 2j), has a phase transition from the rutile-type structure to the $CaCl_2$-type structure at 1 GPa and does not show any phase transition up to 49 GPa at room temperature (Haines et al. 1995). Furthermore, only subtle changes in Raman spectra are expected at the rutile type to the $CaCl_2$ type phase transition, while the changes observed in our study are much more significant (Fig. 2). In addition, if MnO_2 forms at high pressure during measurements, it should remain in the spectra measured for pressure quenched samples. However, we found that the new high-pressure peaks disappear after pressure quench (Fig. 2h, i).

Liu et al. (2002) found a new intense mode in Mn_3O_4 at 600 cm^{-1} at 10 GPa. The wavenumber is close to the most intense mode of the high-pressure phase, N_8, found in our study. However, Liu et al. (2002) found that the new high-pressure mode of Mn_3O_4 remains in the spectra even after pressure quench, while we found that N_8 disappears with decompression (Fig. 2h, i). More importantly, according to our measurements, intense laser illumination on Mn_2O_3 produces MnO_2 not Mn_3O_4 in the diamond-anvil cell.

A synchrotron X-ray diffraction study of Mn_2O_3 by Santillán et al. (2006) showed that the phase transition to the $CaIrO_3$-type structure occurs at 27–38 GPa at room temperature. The pressure interval for the mixed phase region is measured to be 11 GPa indicating a sluggish phase transition at room temperature. New peaks and peak splittings, which are clear evidence for the phase transition, occur at much lower pressures in our Raman measurements, 16–24 GPa.

One possibility is the large difference in the polarizability of bonds between the lower-pressure (C type) and high-pressure ($CaIrO_3$ type) phases. Although the polarizability in the C-type phase is not well known, it has been found that the Raman intensity of the $CaIrO_3$ type is much greater than that of the perovskite type in $MgGeO_3$ (Shim et al. 2007). If the polarizability in the $CaIrO_3$ type is much greater than the C-type structure, it is likely that even small amounts of the high-pressure structure can show up strongly in the Raman spectra of Mn_2O_3, while the low-pressure phase would seem disappear at a lower pressure. In contrast, the X-ray intensity is mainly determined by number of electrons and symmetry. The number of electrons does not change in case of an isochemical phase transition in Mn_2O_3. Therefore, Raman data may provide a

more reliable pressure for the first appearance of the $CaIrO_3$ type in Mn_2O_3.

However, it is also possible that the difference may be caused by experimental conditions. While we use the same pressure medium in the X-ray study (Santillán et al. 2006) and Raman study, as phase transition pressure could be sensitive to stress conditions, a slight difference in stress conditions between the two measurements can contribute to the difference. While we attempted to reduce the heating of the opaque Mn_2O_3 during our Raman measurements (Fig. 1), slight heating of Mn_2O_3 by laser beam can reduce the kinetic effects and therefore stimulate the phase transition at a lower pressure. The diffraction study (Santillán et al. 2006) documented metastable persistence of the $CaIrO_3$-type phase down to 4.5 GPa during decompression. In our Raman study, the most intense peak of the high-pressure phase (N_8) can be observed at 5 GPa (Fig. 2i), consistent with the X-ray observation.

Grüneisen parameters for individual modes (γ_i) can be obtained from the pressure-induced shifts of phonon mode frequencies (Born and Huang 1954; Wallace 1972). We follow the approach presented by Shim et al. (2007) by combining the following two relations:

$$\gamma_i = -\frac{\partial \ln \omega_i}{\partial \ln V}, \tag{1}$$

and

$$\gamma = \gamma_r \left(\frac{V}{V_r}\right)^q, \tag{2}$$

where ω_i is the frequency of mode i, V is volume, q is the logarithmic volume derivative of Grüneisen parameter (γ), which is assumed to be a constant, and subscript r denotes the reference conditions.

Using volume compression data (Santillán et al. 2006) and the second-order Birch–Murnaghan equation, we obtained $K_0 = 144 \pm 5$ GPa for $V_0 = 31.407$ Å^3 for the C-type structure. In case of the $CaIrO_3$-type phase, because it becomes metastable at lower pressures, we set the reference state at 25 GPa where the lowest pressure/volume data point exists for the $CaIrO_3$-type phase in Santillán et al. (2006). This method follows the approach presented by Sata et al. (2002) and Shim et al. (2008) and can reduce uncertainties in the fitting results. We obtained $K_{25GPa} = 231 \pm 20$ GPa for a second-order Birch–Murnaghan equation fit, and the value projected at 1 bar is $K_0 = 127 \pm 20$ GPa. Although the difference in K_0 between the C type and the $CaIrO_3$ type is not statistically significant, it is interesting to note that the $CaIrO_3$-type phase may have the lower bulk modulus. A lower bulk modulus of the post-perovskite ($CaIrO_3$) type compared with a lower-pressure phase (in this case perovskite) was also reported in (Mg,Fe)SiO_3 (Wentzcovitch et al. 2006; Shieh et al. 2006; Shim et al. 2008).

Table 1 Fitting results for the phonon modes of the C type in Mn_2O_3 at 1 bar (ω_0, γ_0, and q) and 25 GPa (γ_{25GPa})

	$\omega_{i,0}$	$\gamma_{i,0}$	q	$\gamma_{i,25GPa}$
n_2	198	1.96 (20)	5.8 (2.0)	0.91
n_3	319	1.03 (3)		1.03
n_4	421	0.50 (3)		0.50
n_5	649	1.38 (5)	0.8 (6)	1.24
n_6	706	1.15 (1)		1.15
$\langle\gamma_i\rangle$		1.20 (53)		0.97 (29)
$\bar{\gamma}$				0.93 (10)

ω_0 for n_4 was obtained from projection of the fitting result to 1 bar, while the other ω_0 values were obtained directly measurements at 1 bar. Except for n_2 and n_5, no significant pressure dependence (q) was resolved for γ_i. Average ($\langle\gamma_i\rangle$) and standard deviation of γ_i are given, together with weighted average following the method by Kieffer (1982), $\bar{\gamma}$

Table 2 Fitting results for the phonon modes of the $CaIrO_3$ type in Mn_2O_3 at 25 GPa ($\omega_{25\ GPa}$, $\gamma_{25\ GPa}$, and q)

	$\omega_{i,25GPa}$	$\gamma_{i,25GPa}$	q
N_1	166	1.42 (10)	
N_2	230	0.90 (8)	
N_3	247	1.04 (7)	
N_4	356	0.72 (5)	
N_5	376	0.94 (5)	
N_6	539	1.19 (26)	
N_7	562	0.79 (3)	
N_8	641	0.76 (3)	
N_9	772	1.23 (10)	6.3 (2.7)
$\langle\gamma_i\rangle$		1.00 (24)	
$\bar{\gamma}$		1.01 (10)	

Except for N_9, no significant pressure dependence (q) was resolved for γ_i. Average ($\langle\gamma_i\rangle$) and standard deviation of γ_i are given, together with weighted average following the method by Kieffer (1982), $\bar{\gamma}$

For the C-type phase, we performed the fitting of the data between 0 and 16 GPa by fixing the wavenumbers of the phonon modes at 1 bar (ω_0) (Table 1). Because n_4 only becomes observable at pressures above 4 GPa, we fit ω_0 together with γ_i in case of n_4. Because n_1 was only observed in a few spectra, we do not perform the fitting for n_1. Except for n_2 and n_5, no significant pressure dependence of mode Grüneisen parameter (q) was found (Table 1).

For the $CaIrO_3$-type phase, we conducted fitting for the data between 25 and 40 GPa (Table 2). Data between 20 and 25 GPa were excluded because of the transient mode shift behaviors observed in this range (Fig. 3). For N_6, because of abrupt changes in the mode shift at 36 GPa, we

did not include the data points near this pressure. The abrupt change might be an artifact due to the difficulty in fitting the weak N_6 at the shoulder of N_7 (Fig. 2). Except for N_9, we did not resolve any pressure dependence of mode Grüneisen parameter. In order to avoid long extrapolation back to 1 bar, we set the reference pressure at 25 GPa for this phase.

We used two different averaging schemes to obtain the spectroscopic Grüneisen parameter (γ_{sp}): simple average ($\langle\gamma_i\rangle$) and a weighted average ($\bar{\gamma}$) following the weighting scheme presented by Kieffer (1982):

$$\bar{\gamma} = \frac{\sum_i C_i \gamma_i}{\sum_i C_i} \tag{3}$$

where C_i is the Einstein heat capacity of the ith mode.

In order to make a more effective comparison of the averaged spectroscopic Grüneisen parameter between the two phases, we calculate the averages at 25 GPa based on the fitting results (Tables 1 and 2). We find that the value of the spectroscopic Grüneisen parameter does not change much with different averaging schemes for the same phase. Although the difference in spectroscopic Grüneisen parameter between the low- and high-pressure phases is not statistically significant, the spectroscopic Grüneisen parameter of the C-type phase (0.93 ± 0.10) is lower than that of the $CaIrO_3$ type (1.01 ± 0.10). This is in contrast to the findings in $MgGeO_3$, $(Mg,Fe)SiO_3$, and $CaIrO_3$ (Shim et al. 2007, 2008; Hustoft et al. 2008) where a decrease in Grüneisen parameter (20–30%) was observed at the perovskite-type to $CaIrO_3$-type transition.

The average Grüneisen parameter for the C-type Mn_2O_3 can also be calculated using the following thermodynamic relationship:

$$\gamma_{th} = \frac{\alpha K_S}{\rho C_P}, \tag{4}$$

where ρ is the density (Geller 1971), C_P is the isobaric heat capacity (Robie and Hemingway 1985), and α is the thermal expansivity obtained from volume data by Grant et al. (1968). K_S is the adiabatic bulk modulus. We obtained the isothermal bulk modulus from Santillán et al. (2006) by fitting the pressure–volume data to the second-order Birch–Murnaghan equation. The difference between adiabatic and isothermal bulk modulus does not normally exceed 5%. From these, we obtained $\gamma_{th} = 3.0 \pm 0.3$, which is significantly larger than the spectroscopic estimation of the Grüneisen parameter for the C type. It is important to note that spectroscopic Grüneisen parameter includes phonon effects only, while the thermodynamic Grüneisen parameter includes all the effects including magnetic behavior. Mn_2O_3 is antiferromagnetic at ambient conditions (Grant et al. 1968). Therefore, it is possible that the large difference is due to unaccounted magnetic effects in the spectroscopic estimation of Grüneisen parameter (γ_{sp}). It is also possible that the discrepancy is due to the detection of only a fraction of Raman-active phonon modes in α-Mn_2O_3. Yet, it is worth noting that good agreement between spectroscopic and thermodynamic Grüneisen parameters has been documented in insulating silicates (Chopelas 1990, 1994) despite the fact that these studies also detect only 10–20% of all the available Raman-active phonon modes. Hofmeister and Mao (2002) proposed that the good agreement is because Raman-active modes are involved in vibrations at the whole unit cell level.

Summary

We report the Raman spectra of the C-type and $CaIrO_3$-type phases in Mn_2O_3 up to 40 GPa under quasi-hydrostatic stress conditions. We detect the phase transition at lower pressures in Raman spectroscopy than in X-ray diffraction, which is, perhaps, due to the larger polarizability of the bonds in the $CaIrO_3$-type structure or experimental factors. The Raman spectra of the $CaIrO_3$ type in Mn_2O_3 are very similar to those of the $CaIrO_3$ type in $MgGeO_3$, while they are different from those of $CaIrO_3$ itself. We estimate the phonon contribution to the Grüneisen parameters of the C type and $CaIrO_3$ type, finding that Grüneisen parameter does not change significantly at the C-type to $CaIrO_3$-type phase transition. The large difference between spectroscopic and thermodynamic Grüneisen parameters in α-Mn_2O_3 (C type) may indicate a large magnetic contribution to the parameter at 1 bar and room temperature.

Acknowledgments We thank two anonymous reviewers for their helpful comments. Construction of the laser Raman system at MIT was supported by NSF (EAR0337156). Raman measurements were supported by NSF for SHS and DL (EAR0337005).

References

Born M, Huang K (1954) Dynamical theory of crystal lattices. Clarendon Press, Oxford

Buciuman F, Patcas F, Craciun R, Zahn DRT (1999) Vibrational spectroscopy of bulk ad supported manganese oxides. Phys Chem Chem Phys 1:185–190

Caracas R, Cohen RE (2006) Theoretical determination of the Raman spectra of $MgSiO_3$ perovskite and post-perovskite at high pressure. Geophys Res Lett 33:L12S05

Catalli K, Shim SH, Prakapenka V (2009) Thickness and Clapeyron slope of the postperovskite transition. Nature 462:782–785

Chopelas A (1990) Thermal properties of forsterite at mantle pressures derived from vibrational spectroscopy. Phys Chem Mineral 17:149–156

Chopelas A (1996) Thermal expansivity of lower mantle phases MgO and $MgSiO_3$ perovskite at high pressure derived from vibrational spectroscopy. Phys Earth Planet Inter 98:3–15

Chopelas A, Boehler R, Ko T (1994) Thermodynamics and behavior of γ-Mg_2SiO_4 at high pressure: Implications for Mg_2SiO_4 phase equilibrium. Phys Chem Mineral 21:351–359

Duan W, Paiva G, Wentzcovitch RM, Fazzio A (1998) Optical transitions in ruby across the corundum to Rh_2O_3 (II) phase transition. Phys Rev Lett 81:3267–3270

Fadini A, Schnepel FM (1989) Vibrational spectroscopy: methods and applications. Halsted Press, Chichester

Funamori N, Jeanloz R (1997) High-pressure transformation of Al_2O_3. Science 278:1109–1111

Geller S (1971) Structures of α-Mn_2O_3, $(Mn_{0.98}Fe_{0.017})_2O_3$ and relation to magnetic ordering. Acta Crystallogr B 27:821–828

Gillet P, Hemley RJ, McMillan PF (1998) Vibrational properties at high pressures and temperature. In: Hemley RJ (eds) Ultrahigh-pressure mineralogy, Reviews in Mineralogy, vol 37. Mineralogical Society of America, pp 525–590

Grant RW, Geller S, Cape JA, Espinosa GP (1968) Magnetic and crystallographic transitions in the α-Mn_2O_3–Fe_2O_3 systems. Phys Rev 175:686–695

Haines J, Léger JM, Hoyau S (1995) Second-order rutile-type to $CaCl_2$-type phase transition in β-MnO_2 at high pressure. J Phys Chem Solid 56:965–973

Hofmeister AM, Mao HK (2002) Redefinition of the mode Grüneisen parameter for polyatomic substances and thermodynamic implications. P Natl Acad Sci 99:559–564

Hustoft J, Shim SH, Kubo A, Nishiyama N (2008) Raman spectroscopy of $CaIrO_3$ postperovskite up to 30 GPa. Am Mineral 93:1654–1658

Kapteijin F, van Langeveld AD, Moulijn JA, Andreini A, Vuurman MA, Turek AM, Jehng JM, Wachs IE (1994) Alumina-supported manganese oxide catalysts. I. characterization: effect of precursor and loading. J Catal 150:94–104

Kieffer SW (1982) Thermodynamics and lattice vibrations of minerals: 5. applications to phase equilibria, isotopic fractionation, and high-pressure thermodynamic properties. Rev Geophys Space Phys 20:827–849

Lin JF, Degtyareva O, Prewitt CT, Dera P, Sata N, Gregoryanz E, Mao HK, Hemley RJ (2004) Crystal structure of a high-pressure/high-temperature phase of alumina by in situ x-ray diffraction. Nat Mater 3:389–393

Liu X, Xu S, Kato K, Moritomo Y (2002) Pressure-induced phase transition in Mn_3O_4 as investigated by Raman spectroscopy. J Phys Soc Jpn 71

Lu R, Hofmeister AM (1994) Thermodynamic properties of ferromagnesium silicate perovskites from vibrational spectroscopy. J Geophys Res 99:11795–11804

Mao HK, Xu J, Bell PM (1986) Calibration of the ruby pressure gauge to 800 kbar under quasihydrostatic conditions. J Geophys Res 91:4673–4676

Murakami M, Hirose K, Kawamura K, Sata N, Ohishi Y (2004) Post-perovskite phase transition in $MgSiO_3$. Science 304:855–858

Oganov AR, Ono S (2004) Theoretical and experimental evidence for a post-perovskite phase of $MgSiO_3$ in Earth's D″ layer. Nature 430:445–448

Oganov AR, Ono S (2005) The high-pressure phase of alumina and implications for Earth's D″ layer. P Natl Acad Sci 102:10828–10831

Ono S, Kikegawa T, Ohishi Y (2004) High-pressure phase transition of hematite, Fe_2O_3. J Phys Chem Solid 65:1527–1530

Piermarini GJ, Glock S, Barnett JD, Forman RA (1975) Calibration of the pressure dependence of the r_1 ruby fluorescence line to 195 kbar. J Appl Phys 46:2774–2780

Prewitt CT, Shannon RD, Rogers DB, Sleight AW (1969) The C rare earth oxide-corundum transition and crystal chemistry of oxides having the corundum structure. Inorg Chem 8:1985–1993

Robie RA, Hemingway BS (1985) Low-temperature molar heat capacities and entropies of MnO_2 (pyrolusite), Mn_3O_4 (hausmanite), and Mn_2O_3 (bixbyite). J Chem Thermodyn 17:165–181

Santillán J, Shim SH, Shen G, Prakapenka VB (2006) High-pressure phase transition in Mn_2O_3—application for the crystal structure and preferred orientation of the $CaIrO_3$ type. Geophys Res Lett 33:L15307

Sata N, Shen G, Rivers ML, Sutton SR (2002) Pressure-volume equation of state of the high-pressure *B*2 phase of NaCl. Phys Rev B 65:104–114

Shieh SR, Duffy TS, Kubo A, Shen G, Prakapenka VB, Sata N, Hirose K, Ohishi Y (2006) Equation of state of the post-perovskite phase synthesized from a natural $(Mg,Fe)SiO_3$ orthopyroxene. P Natl Acad Sci 103:3039–3043

Shim SH, Duffy TS (2002) Raman spectra of Fe_2O_3 to 62 GPa: implications for thermodynamics and phase transformation. Am Mineral 87:318–326

Shim SH, Duffy TS, Jeanloz R, Shen G (2004a) Stability and crystal structure of $MgSiO_3$ perovskite to the core-mantle boundary. Geophys Res Lett 31:L10603

Shim SH, Duffy TS, Jeanloz R, Yoo CS, Iota V (2004b) Raman spectroscopy and x-ray diffraction of phase transitions in Cr_2O_3 to 61 GPa. Phys Rev B 69:144107

Shim SH, Kubo A, Duffy TS (2007) Raman spectroscopy of perovskite and post-perovskite phases of $MgGeO_3$ to 123 GPa. Earth Planet Sc Lett 260:166–178

Shim SH, Catalli K, Hustoft J, Kubo A, Prakapenka VB, Caldwell WA, Kunz M (2008) Crystal structure and thermoelastic properties of $(Mg_{0.91}Fe_{0.09})SiO_3$ postperovskite up to 135 GPa and 2700 K. P Natl Acad Sci 105:7382–7386

Shim SH, Bengtson A, Morgan D, Sturhahn W, Catalli K, Zhao J, Lerche M, Prakapenka VB (2009) Electronic and magnetic structures of the postperovskite-type Fe_2O_3 and implications for planetary magnetic records and deep interiors. P Natl Acad Sci 106:5508–5512

Wallace DC (1972) Thermodynamics of crystals. Wiley, New York

Wentzcovitch RM, Tsuchiya T, Tsuchiya J (2006) $MgSiO_3$ post-perovskite at D″ conditions. P Natl Acad Sci 103:543–546

White WB, Keramidas VG (1972) Vibrational spectra of oxides with the C-type rare earth oxide structures. Spectrochim Acta 28A:501–509

Williams Q, Jeanloz R, McMillan P (1987) Vibrational-spectrum of $MgSiO_3$ perovskite—zero-pressure Raman and midinfrared spectra to 27 GPa. J Geophys Res 92:8116–8128

Yamanaka T, Nagai T, Okada T, Fukuda T (2005) Structure changes of Mn_2O_3 under high pressure and pressure-induced transition. Z Kristallogr 220:938–945